metals

MDPI

Article

Recovering Battery-Grade $LiOH \cdot H_2O$ from Spent Lithium-Containing Sagger Crucible by Thermal Dehydration and $BaSO_4$-Driven Double Decomposition

Seongbong Heo [1] and Jei-Pil Wang [2,*]

[1] Department of Civil and Environmental Engineering, Hanyang University, Seoul 04763, Republic of Korea; well1103@hanyang.ac.kr
[2] Department of Metallurgical Engineering, School of Engineering, Pukyong National University, Busan 48513, Republic of Korea
* Correspondence: jpwang@pknu.ac.kr; Tel.: +82-51-629-6341

Abstract

This study develops and validates an integrated hydrometallurgical process to recover battery-grade lithium hydroxide monohydrate from spent aluminosilicate sagger crucibles. Lithium was first leached as Li_2SO_4 from the crucibles using sulfuric acid; the $Li_2SO_4 \cdot H_2O$ present in the leachate was then thermally decomposed at 300 °C to $Li_2SO_4 + H_2O$, as confirmed by TGA-guided selection and XRD. Subsequent conversion to LiOH proceeded via double decomposition with $Ba(OH)_2$. Guided by HSC-based equilibrium simulations and an Eh–pH analysis of the Li–Ba–S–H_2O system, reaction conditions were optimized over 60–80 °C and $[OH^-]/[Li^+]$ = 1–3. The optimum was identified at 70 °C and $[OH^-]/[Li^+] = 1$, delivering a conversion efficiency of 98.78% and a Li recovery of 98.86%. Two-end-point acid titration indicated a LiOH content of 90.29 wt.% in solution with minimal Li_2CO_3 formation, consistent with processing under vacuum–Ar to suppress CO_2 uptake. The crystallized product obtained by evaporation at ≥90 °C for 24 h was confirmed as $LiOH \cdot H_2O$ (with LiOH) by XRD, while the solid by-product was single-phase $BaSO_4$. ICP-OES measured a final $LiOH \cdot H_2O$ purity of 99.8%.

Keywords: spent sagger crucible; double decomposition; barium hydroxide; $LiOH \cdot H_2O$ purification; $BaSO_4$ precipitation

check for updates

Academic Editors: Petros E. Tsakiridis, Zhongqun Guo and Chenliang Peng

Received: 17 October 2025
Revised: 16 November 2025
Accepted: 19 November 2025
Published: 25 November 2025

Citation: Heo, S.; Wang, J.-P. Recovering Battery-Grade $LiOH \cdot H_2O$ from Spent Lithium-Containing Sagger Crucible by Thermal Dehydration and $BaSO_4$-Driven Double Decomposition. *Metals* **2025**, *15*, 1293. https://doi.org/10.3390/met15121293

Copyright: © 2025 by the authors. Licensee MDPI, Basel, Switzerland. This article is an open access article distributed under the terms and conditions of the Creative Commons Attribution (CC BY) license (https://creativecommons.org/licenses/by/4.0/).

1. Introduction

The global demand for lithium-ion batteries (LIBs) is increasing rapidly, driven primarily by the electrification of transportation and large-scale energy storage deployment. Projections suggest that LIB demand will exceed 4.7 TWh by 2030, highlighting lithium as a critical raw material for achieving carbon neutrality targets [1]. In South Korea, where lithium resources are entirely imported, ensuring a stable supply has become a strategic priority [2]. Consequently, developing cost-effective recycling technologies is imperative to reduce dependence on primary lithium production, mitigate supply chain risks, and support a circular battery economy [3]. Recent studies have identified spent sagger crucibles used in Ni-rich cathode manufacturing as a promising secondary lithium resource [4]. During high-temperature calcination, excess lithium hydroxide reacts with aluminosilicate crucible materials, leading to structural degradation and crack formation. As a result, these crucibles are discarded after limited cycles, with disposal volumes increasing annually. Despite containing approximately 1–2 wt.% lithium in the form of Li–Al–Si–O compounds—comparable

to or exceeding some natural ores such as spodumene ($Li_2O \approx 3.73\%$)—these crucibles are currently pulverized and landfilled after manual removal of residual cathode material [5,6]. This practice not only results in economic losses but also discards a high-grade lithium-bearing resource. Developing recovery methods for such materials can provide a simplified, cost-efficient, and high-yield alternative to conventional ore-based lithium production. Lithium recovery from secondary resources has been extensively investigated through pyrometallurgical processes, which involve high-temperature smelting, roasting, or thermal treatment to decompose lithium-containing phases. For instance, Li et al. [7] reported that lithium can be concentrated in slag phases through high-temperature smelting, enabling subsequent leaching, although significant lithium losses during slag formation remain a challenge. Roasting with additives, such as CaO, Na_2CO_3, or chlorides, has been proposed to convert lithium into more soluble phases, improving leachability [8,9]. However, these approaches are energy-intensive, require complex off-gas treatment, and are often unsuitable for low-lithium-content materials like spent sagger crucibles. Pyro-based hybrid routes, such as roasting followed by leaching, have been applied to improve recovery efficiency from spent cathode materials [10], but similar applications for sagger-derived lithium compounds are scarce, highlighting a critical technological gap. In contrast, hydrometallurgical processes have gained significant attention due to their lower energy requirements, high selectivity, and scalability. These include acid leaching (H_2SO_4, HCl, or organic acids) [11–13], alkaline leaching (NaOH or NH_4OH) for selective phase dissolution [14], and solvent extraction for impurity removal and lithium concentration [15]. Precipitation methods—such as adding Na_2CO_3 or $Ca(OH)_2$—are commonly employed to recover lithium as carbonate or hydroxide with high purity [16]. More recent studies have introduced mechanochemical activation (ball milling with additives) to enhance leachability of refractory lithium phases, achieving up to 90–95% lithium recovery from complex aluminosilicate matrices [17]. Hybrid processes, combining mechanochemical treatment with acid leaching or solvent extraction, have demonstrated improved kinetics and reduced chemical consumption, offering cost-effective alternatives for industrial application [18–20]. Despite these advances, research specifically targeting lithium recovery from spent aluminosilicate sagger crucibles remains limited, necessitating the development of tailored hydrometallurgical and hybrid strategies to address their unique chemical and structural characteristics. In this context, we advance a $Ba(OH)_2$-driven double-decomposition route that converts an industrial Li_2SO_4-rich leachate from spent saggers directly to $LiOH{\cdot}H_2O$ at 60–80 °C. The process is thermodynamically driven by the formation of sparingly soluble $BaSO_4$, achieving near-complete sulfate removal and high LiOH selectivity without a CO_2 loop or intermediate carbonate conversion. Operated under low-CO_2 handling, the route suppresses parasitic Li_2CO_3 formation and tolerates common impurity cations (Al^{3+}, Fe^{3+}, Ca^{2+}, Mg^{2+}), yielding clean LiOH solutions ready for crystallization. Compared with $Ca(OH)_2$ precipitation, $Na_2CO_3 \rightarrow Li_2CO_3 \rightarrow$ LiOH causticization, and direct brine/electrochemical approaches, this offers a short, mild-temperature flowsheet with minimal unit operations and strong compatibility with recycling streams [21–23].

This study aims to develop an efficient process for lithium recovery from spent sagger crucibles. Sulfuric acid leaching was employed to dissolve lithium from the aluminosilicate matrix, followed by selective precipitation to produce lithium hydroxide monohydrate ($LiOH{\cdot}H_2O$). Thermal decomposition of lithium sulfate monohydrate and double-decomposition reactions using barium hydroxide were optimized to maximize lithium conversion. Key parameters, including synthesis temperature and reactant ratios, were investigated. Finally, the recovered $LiOH{\cdot}H_2O$ was dried under vacuum in an Ar atmosphere at 90 °C for 24 h, and the overall lithium recovery efficiency and conversion yield were evaluated to assess the industrial applicability of the proposed method.

2. Materials and Methods

2.1. Experimental Materials

The spent sagger considered here is an alumino-silicate refractory crucible (mullite-based), previously used to hold cathode powders during kiln calcination. Lithium from excess $LiOH/Li_2CO_3$ reacts with the inner wall, leaving Li-bearing Li–Al–Si phases that constitute the Li source recovered in this study. The Li-bearing sulfate solution used in this study was supplied by an industrial partner operating a leaching and purification process for spent aluminosilicate sagger crucibles originating from Li-ion battery cathode production. In this upstream industrial process, the spent saggers are leached under fixed operating conditions of 2.0 mol·L^{-1} H_2SO_4 at a solid-to-liquid ratio of 1:10 (w/v), 80 °C, and 6 h., followed by solid–liquid separation and clarification. These leaching parameters were provided by the industrial facility and are not the subject of optimization or kinetic evaluation in the present work. The clarified Li_2SO_4-rich solution obtained from this process was used as the feed for subsequent $Li_2SO_4 \cdot H_2O$ crystallization, thermal dehydration, and $Ba(OH)_2$ double decomposition experiments.

For the precipitation and double decomposition steps, barium hydroxide ($Ba(OH)_2$, 94–98% purity, analytical grade) was employed as the reactant to convert dissolved Li_2SO_4 into LiOH via $BaSO_4$ formation. All reagents used in this study were of analytical grade and were used without further purification. To minimize contamination and atmospheric CO_2 uptake, samples were subdivided into required amounts inside a glove box, stored in sealed containers, and only opened immediately prior to experimentation. The solid $Li_2SO_4 \cdot H_2O$ precursor obtained from the supplied Li-bearing solution was characterized prior to use. Phase identification was performed by X-ray diffraction (XRD), and elemental composition was analyzed by inductively coupled plasma–optical emission spectrometry (ICP-OES). A representative XRD pattern is shown in Figure 1, and the corresponding chemical composition of the $Li_2SO_4 \cdot H_2O$ feed is summarized in Table 1. These data confirm that $Li_2SO_4 \cdot H_2O$ is the dominant phase, with only minor amounts of Na, Ca, Mg, Si, Fe, and other elements at low levels, which are considered in the assessment of impurity behavior in the subsequent process steps.

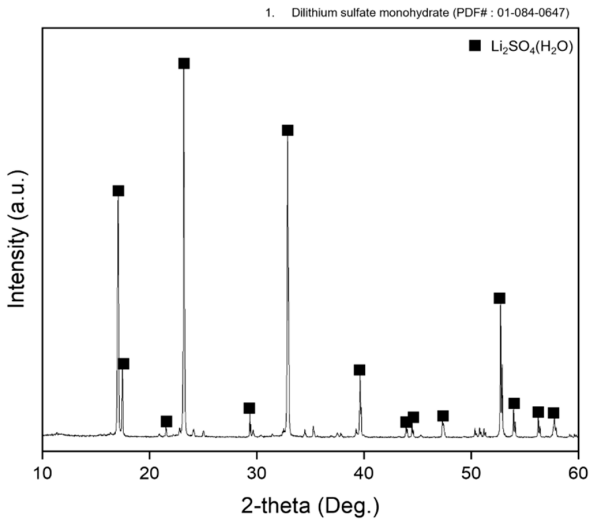


Figure 1. X-ray diffraction (XRD) pattern of the leachate-derived lithium sulfate monohydrate ($Li_2SO_4 \cdot H_2O$) obtained from spent sagger crucibles.

Table 1. Chemical composition of the Li-bearing Li_2SO_4-rich feed solution (25 °C) supplied from industrial leaching of spent sagger crucibles. Values are in $mg \cdot L^{-1}$; pH is reported at 25 °C. Elements not listed were below the instrumental detection limit (<0.001 $mg \cdot L^{-1}$).

Element/Parameter	Concentration ($mg \cdot L^{-1}$) or Value
pH (25 °C)	9.48
Li	1373
Na	1830.44
Ca	21.638
Mg	3.042
Si	21.159
Fe	2.017

Trace elements (<0.001 $mg \cdot L^{-1}$): Pb, Co, Cr, Cu, K, Mn, Yb, Sm, Mo, Be, Bi, Cd, Sb, Se, Tm, Th, Ni, Tb, Sc, Ag, Al, As, B.

2.2. Experimental Apparatus

The thermal decomposition of lithium sulfate monohydrate ($Li_2SO_4 \cdot H_2O$) was performed in an argon (Ar)-purged glove box to prevent oxidation and contamination. The schematic of the glove box system is shown in Figure 2a. The concentrations of O_2 (g) and H_2O (g) inside the glove box were monitored using built-in gas sensors and maintained at 37.1 ppm and 0.36 ppm, respectively, to ensure a controlled inert atmosphere. A heater was installed beneath the reactor, and a thermocouple was attached directly to the crucible to measure the reactor's internal temperature. The temperature was regulated via a precision temperature controller connected to the thermocouple. After thermal decomposition, the recovery of lithium hydroxide monohydrate ($LiOH \cdot H_2O$) from the leachate was conducted using the apparatus illustrated in Figure 2b. Barium hydroxide ($Ba(OH)_2$) was employed as the precipitating agent to induce a double decomposition reaction between $Li_2SO_4 \cdot H_2O$ and $Ba(OH)_2$, producing $LiOH \cdot H_2O$ while precipitating barium sulfate ($BaSO_4$). To prevent the conversion of LiOH to lithium carbonate (Li_2CO_3) caused by reaction with atmospheric CO_2, the reaction was carried out under a vacuum Ar atmosphere using a Teflon vacuum pump. The lithium sulfate solution was loaded into a separatory funnel, and after purging the system with Ar to stabilize the internal atmosphere, the solution was released into a Teflon beaker. Teflon vessels were chosen to prevent the formation of lithium silicate (Li_2SiO_3), which can occur when using glass containers. The solution and $Ba(OH)_2$ were stirred at the desired reaction temperature using a magnetic bar driven by the heating mantle's magnetic field to promote uniform reaction. The separation of the resulting $LiOH \cdot H_2O$ solution and $BaSO_4$ precipitate was achieved via vacuum filtration using the setup depicted in Figure 2c. A PTFE-hydrophilic membrane filter with a pore size of 0.2 µm was used to effectively separate the solid precipitates. The filtered LiOH solution was subsequently dried under vacuum–Ar conditions at 90 °C to prevent CO_2 uptake and obtain high-purity $LiOH \cdot H_2O$. This approach avoided the undesired formation of Li_2CO_3, which typically occurs during atmospheric evaporation. Thermal dehydration converts $Li_2SO_4 \cdot H_2O \rightarrow Li_2SO_4 + H_2O(g)$, eliminating waters of crystallization and adventitious moisture/CO_2. This standardizes the feed as anhydrous Li_2SO_4, prevents HSO_4^- formation and OH^- overconsumption during heating, and allows accurate control of the $[OH^-]/[Li^+]$ ratio and Li/SO_4^{2-} mass balance when the solid is later re-dissolved for the $Ba(OH)_2$ double-decomposition step.

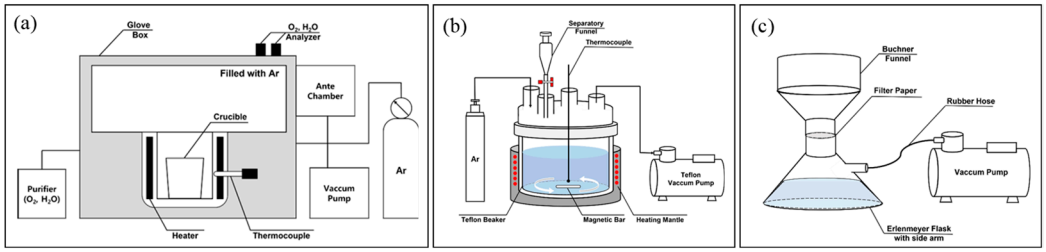


Figure 2. Integrated schematic of the experimental workflow used in this study: (**a**) argon-purged glove-box furnace for thermal dehydration of $Li_2SO_4 \cdot H_2O$ in an MgO crucible; (**b**) $Ba(OH)_2$ double-decomposition reactor; and (**c**) vacuum filtration of the $BaSO_4$ precipitate using a PTFE membrane (0.2 µm) to obtain the LiOH solution for subsequent crystallization.

2.3. Overall Process Flow

The overall process for recovering lithium hydroxide monohydrate ($LiOH \cdot H_2O$) from spent sagger crucibles is illustrated in Figure 3. The process consists of four major steps: 1—Leaching: Lithium in spent aluminosilicate sagger crucibles is dissolved using sulfuric acid to produce a leachate primarily containing lithium sulfate monohydrate ($Li_2SO_4 \cdot H_2O$); 2—Thermal Decomposition: The leachate is subjected to controlled heating to decompose $Li_2SO_4 \cdot H_2O$ into anhydrous lithium sulfate (Li_2SO_4), releasing structural water; 3—Double Decomposition and Precipitation: Barium hydroxide ($Ba(OH)_2$) is added to the decomposed lithium sulfate solution under a vacuum–argon atmosphere, leading to the formation of $LiOH \cdot H_2O$ while precipitating $BaSO_4$; 4—Drying and Purification: The lithium hydroxide solution is dried under vacuum at 90 °C in an argon-purged environment to prevent carbonation, yielding high-purity $LiOH \cdot H_2O$. This flow ensures high lithium recovery efficiency while minimizing unwanted side reactions and the formation of lithium carbonate due to atmospheric CO_2 exposure.

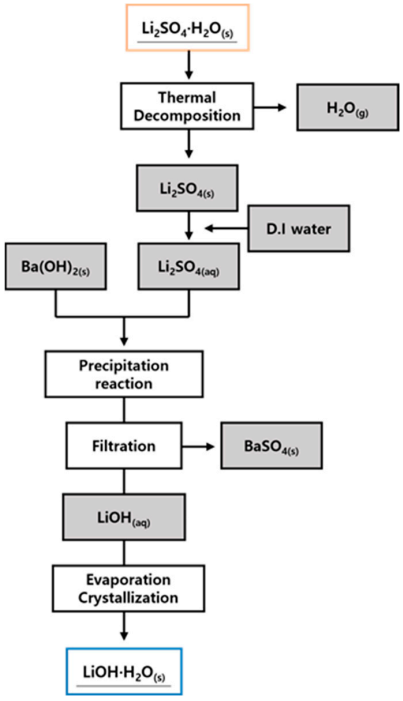


Figure 3. Overall flowsheet for producing $LiOH \cdot H_2O$ from an industrial Li_2SO_4-rich leachate of spent saggers. The key precipitation (double-decomposition) step is: $Li_2SO_4(aq) + Ba(OH)_2(aq) \rightarrow 2\ LiOH(aq) + BaSO_4(s)$, operated at 60–80 °C with $[OH^-]/[Li^+] = 1$–3 (optimum ≈ 1) under a vacuum–Ar headspace to suppress CO_2 uptake. Sparingly soluble $BaSO_4(s)$ provides the thermodynamic driving force for sulfate removal, after which the LiOH solution is crystallized to $LiOH \cdot H_2O$.

2.4. Thermal Dehydration of $Li_2SO_4 \cdot H_2O$

Thermodynamic screening was performed using HSC Chemistry (version 9) to identify feasible dehydration conditions; detailed outcomes are presented in Section 3.1. Thermal dehydration experiments were conducted in MgO crucibles (selected based on chemical-compatibility assessment) under flowing argon. Samples of $Li_2SO_4 \cdot H_2O$ were heated in a thermogravimetric analyzer at 5 °C·min^{-1} to the target temperature and held isothermally for 30 mins. Phase identification before and after heating was performed by X-ray diffraction (XRD). The overall dehydration reaction considered in this work is summarized in Section 3.1.

2.5. $Ba(OH)_2$ Double Decomposition Experiments

Li_2SO_4 solutions were prepared at 0.10 mol·L^{-1} from the supplied Li-bearing feed. Barium hydroxide [$Ba(OH)_2$, analytical grade] was used as the precipitant for the double decomposition step. Experiments were carried out in sealed Teflon vessels under continuous stirring at 60, 70, or 80 °C, with the molar ratio [OH^-]/[Li^+] = 1.0, 2.0, or 3.0 adjusted by the $Ba(OH)_2$ addition. After reaction, suspensions were filtered to collect the $BaSO_4$ solids and the Li-containing filtrate. Solution pH and redox potential (Eh) were measured. Quantitative definitions and equations for conversion, Li recovery, and titration-based phase fractioning (LiOH vs. Li_2CO_3) are consolidated and All quantitative results and interpretations are reported.

2.6. $Ba(OH)_2$ Double Decomposition Experiments

To investigate the precipitation and double displacement reaction between Li_2SO_4 solution and $Ba(OH)_2$, a series of experiments were conducted under various conditions. The reaction temperatures were selected based on the equilibrium composition, specifically 60 °C, 70 °C, and 80 °C. The molar ratio of hydroxide ions to lithium ions ([OH^-]:[Li^+]) was varied at 1:1, 2:1, and 3:1 to evaluate the influence of excess OH^- on the precipitation behavior. The initial Li_2SO_4 concentration was maintained at 0.1 M, corresponding to an initial lithium concentration of 1373 ppm and an initial pH of 9.48. The detailed experimental conditions are summarized in Table 2.

Table 2. Experimental conditions for the precipitation and double displacement reaction between Li_2SO_4 and $Ba(OH)_2$, including temperature and molar ratio of [OH^-] to [Li^+].

Li_2SO_4 Conc.	Initial Li Conc.	Initial pH	Temperature, °C	[OH]:[Li]
0.1 M	1373 ppm	9.48	60	1:0.1
				2:0.1
				3:0.1
			70	1:0.1
				2:0.1
				3:0.1
			80	1:0.1
				2:0.1
				3:0.1

To evaluate the efficiency of the conversion reaction from lithium sulfate to lithium hydroxide, the conversion rate was calculated based on the concentration of sulfate ions (SO_4^{2-}) remaining in the filtrate after the reaction. The following equation was used to determine the conversion rate shown in Equation (1):

$$Conversion\ rate\ (\%) = [1 - \frac{m_{SO_4^{2-},\ after}}{m_{SO_4^{2-},\ initial}}] \times 100 \quad (1)$$

where $m_{SO_4^{2-},\,after}$: the amount of SO_4^{2-} ions remaining in the solution after the reaction, $m_{SO_4^{2-},\,initial}$: the amount of SO_4^{2-} ions initially present in the Li_2SO_4 solution.

3. Results and Discussion

3.1. Thermal Decomposition of Lithium Sulfate Monohydrate

Prior to the thermal decomposition experiments, thermodynamic equilibrium analysis was conducted using HSC Chemistry (Outotec, version 9) to determine the onset temperature for the dehydration of lithium sulfate monohydrate ($Li_2SO_4{\cdot}H_2O$). As shown in Figure 4, the decomposition reaction begins at approximately 130 °C, following Equation (2);

$$Li_2SO_4{\cdot}H_2O(s) \rightarrow Li_2SO_4(s) + H_2O(g) \quad (2)$$

The equilibrium analysis indicated that dehydration is accompanied by a continuous increase in the entropy of the system, consistent with the phase transition of water from solid to vapor. The decomposition does not generate additional reactive intermediates that would interfere with subsequent reactions with barium hydroxide. The calculated standard Gibbs free energy change (ΔG°) for this reaction decreases with temperature, reaching approximately -12.3 kJ·mol^{-1} at 300 °C, confirming that the dehydration process is thermodynamically favorable at the selected experimental temperature. The enthalpy change (ΔH°) for the reaction was estimated at +44.2 kJ·mol^{-1}, reflecting the endothermic nature of water release, while the entropy change (ΔS°) was approximately +187 J·mol^{-1}·K^{-1}, supporting the spontaneous progression at elevated temperatures.

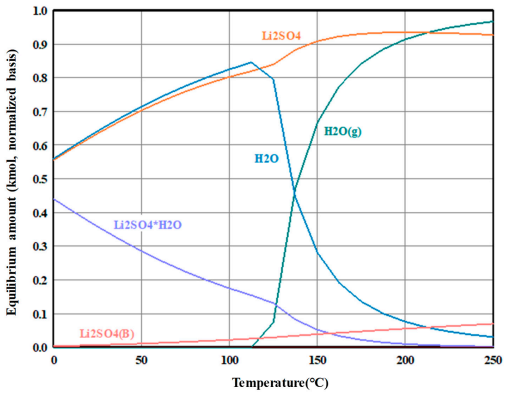


Figure 4. Thermodynamic equilibrium composition of the $Li_2SO_4{\cdot}H_2O$ decomposition reaction obtained using HSC Chemistry, showing the onset of dehydration at approximately 130 °C.

Considering the decomposition profile and the melting point of anhydrous lithium sulfate (859 °C), thermogravimetric analysis (TGA) was conducted under an argon atmosphere to validate the simulation results (Figure 5). The sample was heated at a rate of 5 °C·min^{-1} up to 600 °C and held for 30 min to monitor mass changes during decomposition. The TGA results showed a significant weight loss starting at approximately 130 °C, consistent with the HSC thermodynamic predictions, corresponding to the release of structural water. Based on these results, an experimental decomposition temperature of 300 °C was selected to ensure complete dehydration while minimizing unwanted side reactions.

The compatibility between the decomposing lithium sulfate and potential crucible materials (MgO and Al_2O_3) was also evaluated using HSC thermodynamic simulations. As shown in Figure 6, MgO crucibles exhibited negligible reactivity with Li_2SO_4 across the studied temperature range, with no intermediate phases forming. In contrast, Al_2O_3 crucibles (Figure 7) showed the formation of $LiAlO_2$ as a secondary phase, with its amount increasing at higher temperatures. The formation of $LiAlO_2$ can reduce the effective lithium

recovery and interfere with the subsequent double decomposition reaction with barium hydroxide. Therefore, MgO crucibles were selected as the optimal reaction vessels for the thermal decomposition experiments due to their superior chemical stability and inertness toward lithium sulfate.

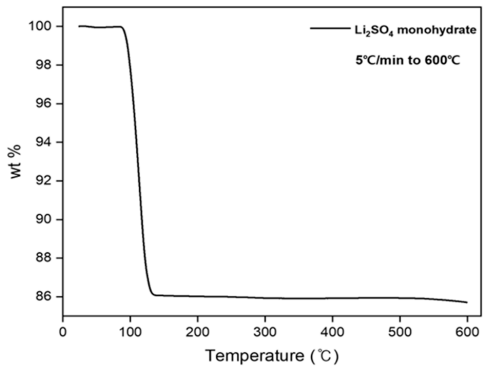


Figure 5. Thermogravimetric analysis (TGA) curve of $Li_2SO_4 \cdot H_2O$ under an argon atmosphere, heated at 5 °C·min^{-1} to 600 °C and held for 30 min, confirming weight loss due to dehydration.

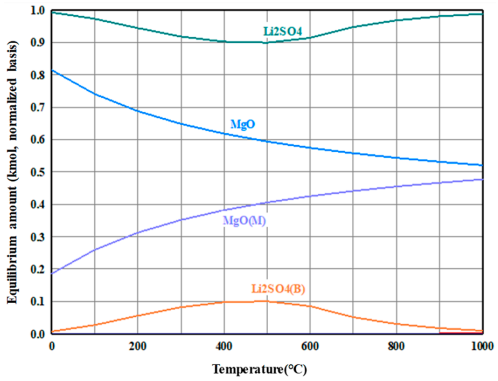


Figure 6. Equilibrium phase composition of Li_2SO_4 with MgO crucible material as a function of temperature, indicating no reactive phase formation.

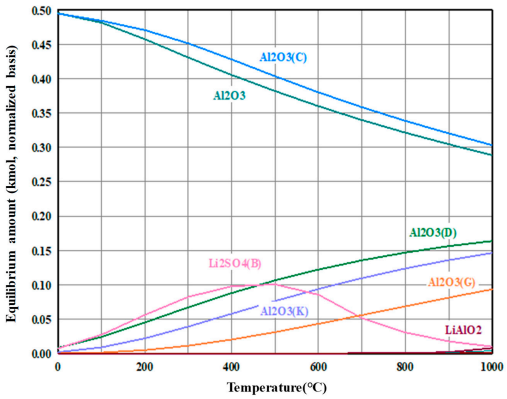


Figure 7. Equilibrium phase composition of Li_2SO_4 with MgO crucible material as a function of temperature, indicating no reactive phase formation.

3.2. Precipitation and Double Decomposition Reaction

To recover lithium hydroxide monohydrate ($LiOH \cdot H_2O$) from the leachate, the precipitation reaction was carried out through a double decomposition process using various precipitants. The lithium content in the leachate obtained from sulfuric acid roasting of spent aluminosilicate sagger crucibles was estimated to be approximately 1000–4000 ppm, depending on the cathode material processed in the saggers. Based on this range, the

concentration of lithium sulfate (Li_2SO_4) solution was fixed at 0.1 mol·L^{-1} for the experiments. Barium hydroxide [$Ba(OH)_2$] was selected as the primary precipitant due to its high selectivity for lithium hydroxide formation and the low solubility of the byproduct barium sulfate ($BaSO_4$), which facilitates efficient phase separation. Experiments were performed by varying the molar ratio of $Ba(OH)_2$ to Li_2SO_4 and the reaction temperature to optimize the double decomposition efficiency. To better understand the dissolution behavior of Li_2SO_4 in deionized water and its interaction with $Ba(OH)_2$, thermodynamic equilibrium simulations were conducted using HSC Chemistry (Outotec, version 6). As shown in Figure 8, lithium sulfate undergoes stepwise ionization when dissolved in deionized water. At ambient temperature, Li_2SO_4 partially dissociates into Li^+ and $LiSO_4^-$ ions, following Equation (3). With increasing temperature, particularly above 65 °C, complete ionization into Li^+ and SO_4^{2-} occurs, as described by Equation (4).

$$Li_2SO_4 \rightarrow Li^+ + LiSO_4^- \quad (3)$$

$$LiSO_4^- \rightarrow Li^+ + SO_4^{2-} \quad (4)$$

Above 70 °C, the interaction between SO_4^{2-} ions and water molecules leads to secondary acid–base equilibria that generate bisulfate and hydroxide, as shown in Equation (5):

$$SO_4^{2-} + H_2O \rightarrow HSO_4^- + OH^- \quad (5)$$

This equilibrium indicates that elevated temperature enhances OH^- availability in solution, which in turn facilitates the $Ba(OH)_2$-driven precipitation of $BaSO_4$ and the formation of LiOH. These findings suggest that operating the precipitation step at elevated temperatures (>70 °C) improves ion availability and enhances the overall efficiency of lithium hydroxide formation. Consequently, the reaction conditions for the double decomposition were optimized considering both thermodynamic predictions and experimental results.

Although the solubility of lithium sulfate (Li_2SO_4) suggests that it can readily dissolve at ambient temperature, thermodynamic analysis indicates that the degree of lithium ionization at room temperature is insufficient for effective participation in the double decomposition reaction. To ensure complete ionization and maximize reactivity with barium hydroxide, the lithium sulfate solution was therefore prepared at 65–75 °C. As illustrated in Figure 9, when the Li_2SO_4 solution was reacted with $Ba(OH)_2$, the equilibrium composition simulations revealed that at 25–55 °C, products such as LiOH, $LiOH{\cdot}H_2O$, and $BaSO_4$ were formed. However, these reactions likely occurred under conditions of incomplete ionization, resulting in slower kinetics and reduced efficiency. In contrast, operating above 80 °C led to the formation of undesirable byproducts, such as HSO_3^-, altering the stoichiometry of reactive ions. Therefore, to achieve a balance between complete ionization and minimal side reactions, the optimal reaction temperature range was set to 60–80 °C, which ensures efficient ion availability for the double decomposition process while preventing the onset of secondary reactions.

Once lithium sulfate (Li_2SO_4) is fully ionized, the ions interact to form solid compounds containing one type of cation and one type of anion. Based on solubility predictions, barium sulfate ($BaSO_4$) is a highly insoluble sulfate, which thermodynamically drives the double decomposition reaction as represented in Equation (6).

$$Li_2SO_4(aq) + Ba(OH)_2(aq) \rightarrow 2LiOH(aq) + BaSO_4(s) \quad (6)$$

The Eh–pH diagram for the Li–Ba–S–H_2O system at 70 °C is shown in Figure 10, illustrating the stability domains of the relevant phases. LiOH(aq) is stable in the alkaline region above pH 12, confirming that the addition of $Ba(OH)_2$ to the Li_2SO_4 solution

increases pH sufficiently to favor LiOH formation while simultaneously precipitating $BaSO_4$. To validate these predictions, the Eh and pH of the filtrated LiOH solution (after $BaSO_4$ removal) were measured, confirming that the solution conditions corresponded to the LiOH stability domain predicted by the thermodynamic model.

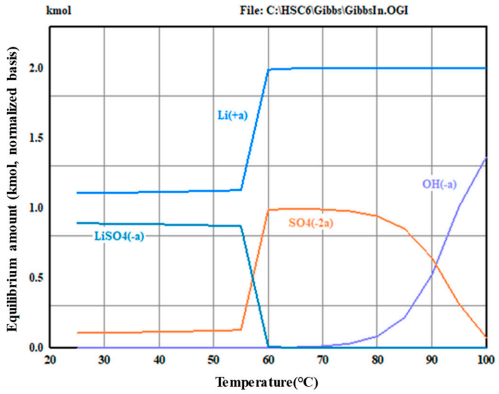


Figure 8. Equilibrium composition of Li_2SO_4 in deionized water as a function of temperature, simulated using HSC Chemistry (Outotec, version 6).

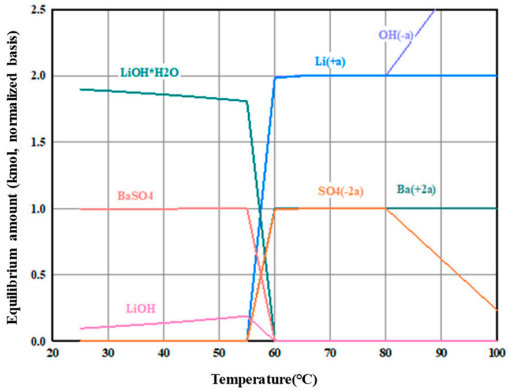


Figure 9. Thermodynamic equilibrium composition of the double decomposition reaction between Li_2SO_4 and $Ba(OH)_2$ as a function of temperature.

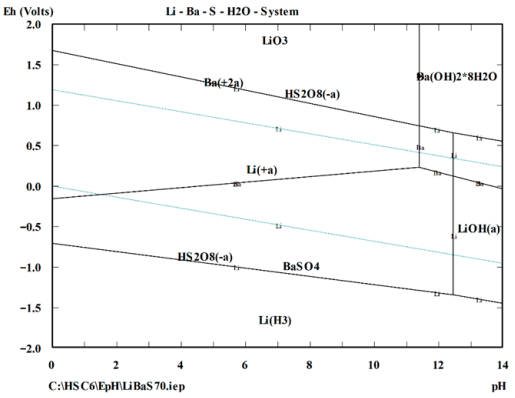


Figure 10. Eh–pH diagram of the Li–Ba–S–H_2O system at 70 °C, showing the stability fields of LiOH(aq), $BaSO_4$(s), and other relevant species.

3.3. Thermal Decomposition of Lithium Sulfate Monohydrate

To evaluate whether the thermal decomposition of lithium sulfate monohydrate ($Li_2SO_4 \cdot H_2O$) occurs spontaneously, the Gibbs free energy change (ΔG) and equilibrium constant (K) of the reaction were calculated as functions of temperature. The decomposition reaction is expressed as

$$Li_2SO_4 \cdot H_2O(s) \rightarrow Li_2SO_4(s) + H_2O(g) \quad (7)$$

The Gibbs free energy at non-standard states is expressed as:

$$\Delta G = \Delta G^\circ + RT\ln Q \quad (8)$$

At equilibrium, Q = K and ΔG = 0, giving:

$$\Delta G^\circ = -RT\ln K \quad (9)$$

$$K = e^{\{-\{\Delta G^\circ\}/\{RT\}\}} \quad (10)$$

The standard-state Gibbs free energy change for the reaction is calculated as

$$\Delta G^\circ_{rxn} = \Delta H^\circ_{rxn} - T\Delta S^\circ_{rxn} \quad (11)$$

The temperature dependence of enthalpy and entropy is expressed as:

$$\Delta H^\circ(T) = \Delta H^\circ_{rxn}(298.15K) + \int_{298.15K}^{T} C_p dT \quad (12)$$

$$\Delta S^\circ(T) = \Delta S^\circ_{rxn}(298.15K) + \int_{298.15K}^{T} \frac{\Delta C_p}{T} dT \quad (13)$$

Thus, the Gibbs free energy at temperature T is:

$$\Delta G^\circ(T) = \left[\Delta H^\circ_{rnx} + \Delta C_p(T - 298.15K)\right] - T\left[\Delta R^\circ_{rnx} + \Delta C_p \ln\left(\frac{T}{298.15K}\right)\right] \quad (14)$$

Using Equations (7)–(14), the temperature-dependent Gibbs free energy and equilibrium constant K were calculated, as shown in Figure 11. The results indicate that the equilibrium constant *K* increases with temperature, while the Gibbs free energy decreases, becoming negative above approximately 300 °C. This confirms that the decomposition of $Li_2SO_4 \cdot H_2O$ to Li_2SO_4 and H_2O is thermodynamically spontaneous under the selected experimental conditions.

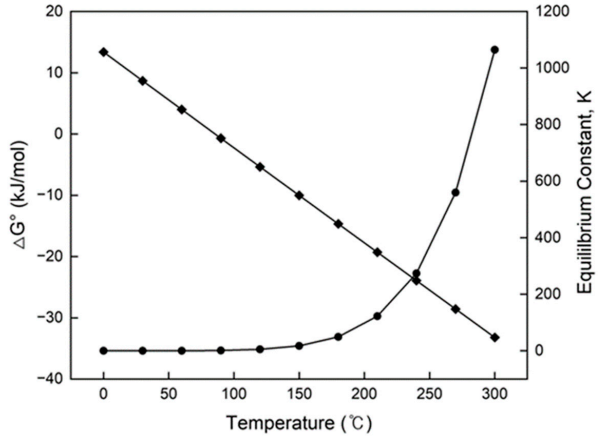


Figure 11. Temperature dependence of the standard Gibbs free energy change (ΔG°) and equilibrium constant (K) for the thermal decomposition of $Li_2SO_4 \cdot H_2O$, calculated using Equations (7)–(11).

To confirm the removal of crystal water from lithium sulfate monohydrate ($Li_2SO_4 \cdot H_2O$), a thermal decomposition experiment was carried out at 300 °C under an argon (Ar) atmosphere using a glove box. The decomposition temperature was selected based on predictions from HSC Chemistry equilibrium composition simulations and thermogravimetric analysis

(TGA). After thermal treatment, the decomposition products were analyzed using X-ray diffraction (XRD), as shown in Figure 12.

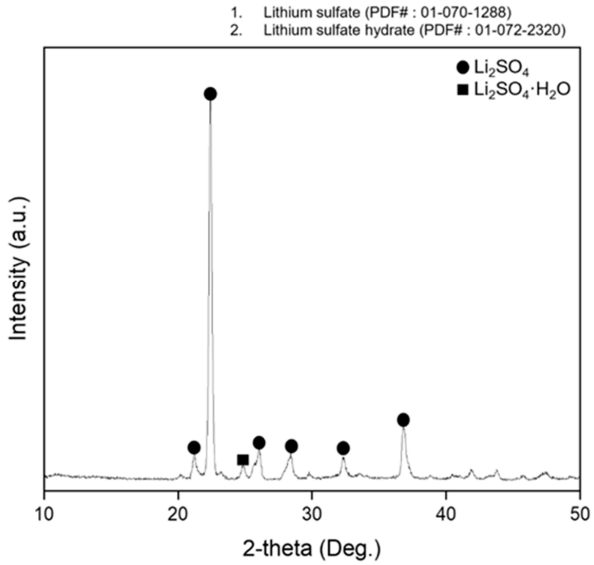


Figure 12. XRD pattern of the thermally decomposed product at 300 °C, showing the transformation of $Li_2SO_4 \cdot H_2O$ into Li_2SO_4.

The XRD results indicated that $Li_2SO_4 \cdot H_2O$ was successfully converted to anhydrous Li_2SO_4 at 300 °C, confirming the removal of crystal water. Moreover, the absence of any secondary phases implied that the Li_2SO_4 product did not react with the MgO crucible. Elemental analysis (EA) results, summarized in Table 3, further validated the dehydration reaction. The reduction in hydrogen (H) content and the significant decrease in oxygen (O) content were consistent with the theoretical mass loss associated with the release of one molecule of H_2O, in agreement with the TGA data. In addition, the XRD pattern revealed that while the majority of the $Li_2SO_4 \cdot H_2O$ phase had been replaced by Li_2SO_4, a small residual amount of $Li_2SO_4 \cdot H_2O$ still remained. This is likely due to the partial rehydration of the thermally decomposed Li_2SO_4 product upon exposure to ambient moisture during handling and sample transfer for XRD measurement outside the glove box. Nevertheless, the obtained Li_2SO_4 was used in the subsequent recovery process without further purification.

Table 3. Elemental analysis (EA) results for $Li_2SO_4 \cdot H_2O$ and the thermally decomposed Li_2SO_4.

Element	Raw $Li_2SO_4 \cdot H_2O$, wt.%	Thermal Decomposition Li_2SO_4, wt.%
H	0.756	–
O	50.886	37.503

3.4. Precipitation and Double Displacement Reaction

As shown in Figure 13, conversion experiments were conducted at three different molar ratios of $[OH^-]/[Li^+]$ (1:1, 2:1, and 3:1) under varying temperature conditions (60 °C, 70 °C, and 80 °C). All data points represent the mean of $n = 3$ independent experiments. The dispersion among replicates was within the measurement precision and therefore smaller than the symbol size in Figures 13–16. The results demonstrated that more than 90% conversion was achieved in all molar ratio conditions. However, a decreasing trend in conversion rate was observed with increasing $[OH^-]/[Li^+]$ ratio. This is attributed to stoichiometric limitations, where excess hydroxide ions do not further contribute to conversion and may instead hinder precipitation efficiency. Furthermore, it was observed

that lower temperatures resulted in slightly reduced conversion rates, which is likely due to the lower solubility and slower dissolution rate of $Ba(OH)_2$ at lower temperatures. As the availability of Ba^{2+} ions in solution is limited under such conditions, the overall ion-exchange and precipitation kinetics are suppressed [19,20].

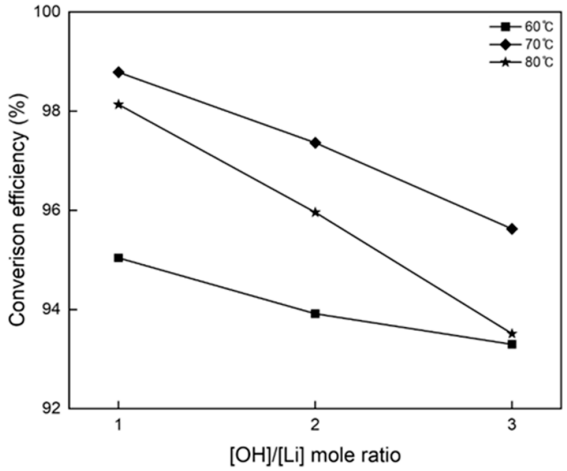


Figure 13. Conversion rate of Li_2SO_4 to LiOH as a function of $[OH^-]/[Li^+]$ molar ratio and temperature. The conversion was evaluated based on the reduction of SO_4^{2-} ions in solution after the reaction.

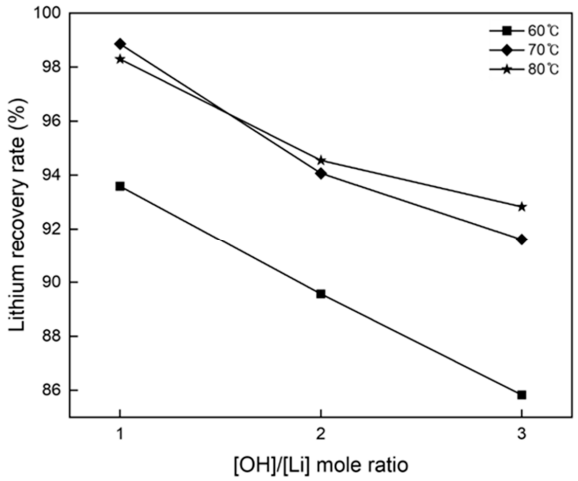


Figure 14. Effect of $[OH^-]/[Li^+]$ molar ratio and temperature on lithium recovery from Li_2SO_4 solution.

Figure 14 illustrates the lithium recovery efficiency from the solution after the precipitation and double displacement reaction, conducted under varying $[OH^-]/[Li^+]$ molar ratios and temperatures. The lithium recovery yield was calculated using Equation (15):

$$Li\ recovery\ yield\ (\%) = \left(\frac{Recoverd\ Li}{Li\ content\ in\ Li_2SO_4 \cdot H_2O}\right) \quad (15)$$

where V_t is the residual voltage at final time t and V_0 is the initial voltage.

Here, the lithium content in the raw material ($Li_2SO_4 \cdot H_2O$) was obtained by multiplying the total weight of the sample by the lithium content percentage. The recovered lithium amount was calculated based on the weight of $LiOH \cdot H_2O$ obtained after filtration and its lithium content. This calculation ensures accurate quantification of lithium mass recovery following the $Ba(OH)_2$-induced precipitation reaction.

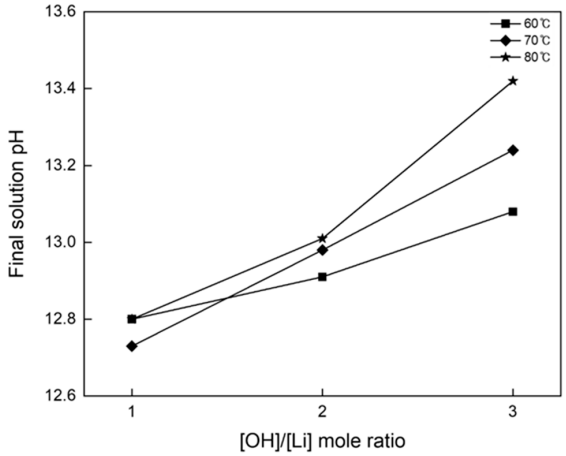


Figure 15. Measured pH values of the recovered LiOH solutions under varying $[OH^-]/[Li^+]$ molar ratios at 60, 70, and 80 °C.

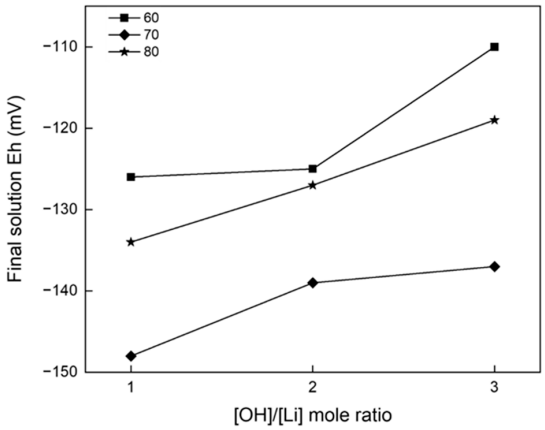


Figure 16. Measured Eh values of the recovered LiOH solutions under the same experimental conditions.

Experimental results revealed that the lithium recovery yield increased with temperature, indicating enhanced recovery at higher temperatures. In contrast, as the $[OH^-]/[Li^+]$ molar ratio increased from 1:1 to 3:1, the recovery yield tended to decrease. This inverse relationship can be attributed to the increased viscosity of the reaction medium caused by the excess $Ba(OH)_2$ and formation of $BaSO_4$ precipitate. Higher solution viscosity hampers the filtration process by reducing the permeability of the reaction mixture, as explained by Darcy's law. Additionally, at elevated temperatures, the solubility and dissolution rate of $Ba(OH)_2$ increase, which accelerates the formation of LiOH and facilitates more efficient solid–liquid separation, ultimately improving the recovery efficiency. These findings confirm that optimizing both the reaction temperature and molar ratio is crucial for maximizing lithium recovery from Li_2SO_4-based solutions. The pH and Eh of the recovered LiOH solution were measured under varying $[OH^-]/[Li^+]$ molar ratios and reaction temperatures. As shown in Figures 17 and 18, both parameters were assessed to evaluate the electrochemical stability and compositional behavior of the final solution. The results were further interpreted based on the thermodynamic boundaries presented in the Eh–pH diagram of the Li–Ba–S–H_2O system (Figure 10).

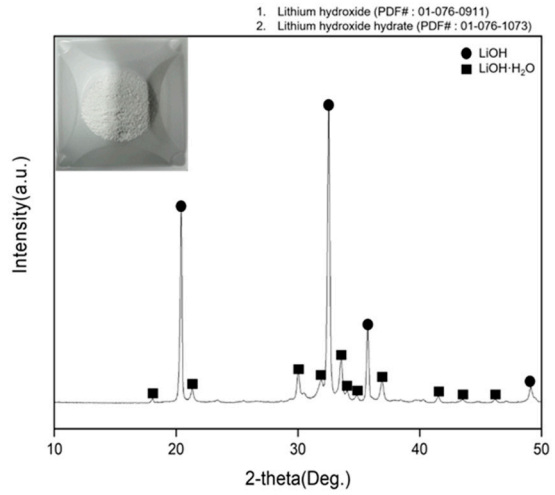


Figure 17. X-ray diffraction (XRD) pattern of the lithium hydroxide product crystallized by vacuum–argon evaporation at ≥90 °C for 24 h.

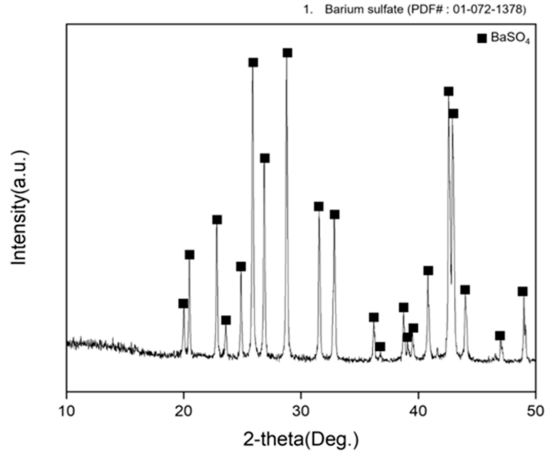


Figure 18. X-ray diffraction (XRD) pattern of the post-filtration precipitate, confirming single-phase $BaSO_4$ formation, which evidences the selectivity and driving force of the $Ba(OH)_2$-assisted double decomposition route.

As the $[OH^-]/[Li^+]$ molar ratio increased, the pH of the LiOH solution exhibited a corresponding increase. This behavior is attributed to the progressive dissociation of OH^- ions from $Ba(OH)_2$, which directly contributes to the alkalinity of the system. Notably, the measured pH values at all reaction conditions fell within the aqueous stability field of LiOH(aq) on the Eh–pH diagram, confirming that the resulting solutions are thermodynamically consistent with the target LiOH phase. Conversely, the Eh values showed negligible variation across different molar ratios and temperatures, remaining within a narrow potential window. This thermodynamic stability implies that the redox environment of the system was not significantly influenced by the precipitation of $BaSO_4$ or excess $Ba(OH)_2$. More importantly, all experimental points were located below the oxygen evolution line and above the hydrogen evolution line, indicating that water electrolysis or redox decomposition did not occur. This observation confirms that the redox conditions were maintained in the non-corrosive and electrochemically stable region, preventing the formation of unwanted species such as elemental sulfur or sulfides. Furthermore, the alignment of experimental data within the thermodynamic stability domain of LiOH(aq) in the Li–Ba–S–H_2O system provides strong evidence that the $Ba(OH)_2$-assisted precipitation process not only enhances sulfate removal but also facilitates the selective recovery of Li as a chemically stable hydroxide product. Table 4 summarizes the experimental results for

lithium concentration (Li ppm), residual sulfate concentration (SO_4^{2-} ppm), conversion efficiency, and lithium recovery under varying [OH]/[Li] molar ratios (1:1, 2:1, 3:1) and temperatures (60 °C, 70 °C, and 80 °C). The conversion efficiency was calculated based on the decrease in SO_4^{2-} ion concentration before and after the reaction using Equation (16), while lithium recovery was calculated using Equation (17), which considers the Li content in recovered LiOH relative to the theoretical amount in the starting material. As the reaction temperature increased, both the conversion efficiency and Li recovery generally improved. At 70 °C, the highest conversion efficiency of 98.784% and Li recovery of 98.86% were achieved under the [OH]/[Li] = 1:1 condition, indicating this to be the optimal reaction condition within the tested range. In contrast, increasing the [OH]/[Li] molar ratio beyond stoichiometric amounts (i.e., 2:1 and 3:1) led to a gradual decrease in both conversion and recovery. This trend is attributed to the excessive addition of $Ba(OH)_2$, which increases the viscosity of the solution due to the formation of residual unreacted $Ba(OH)_2$ and $BaSO_4$ precipitates. Elevated viscosity likely hinders the diffusion of reactants and products, as well as impairing filtration efficiency, thereby reducing the effective Li recovery despite high conversion values. This behavior is in agreement with thermodynamic expectations, as stoichiometric balance minimizes unnecessary side reactions and solid phase formation, promoting efficient conversion of Li_2SO_4 to LiOH.

Table 4. Experimental results of lithium concentration, residual SO_4^{2-} concentration, conversion efficiency, and lithium recovery as a function of [OH]/[Li] molar ratio and reaction temperature.

[OH]:[Li]	Temperature, °C	Li, ppm	SO_4, ppm	Conversion Efficiency, %	Li Recovery Rate, %
1:0.1	60	1947.40	9.13	95.04	93.59
2:0.1		1874.92	11.27	93.91	89.57
3:0.1		1832.0	12.66	93.29	85.83
1:0.1	70	2886.13	3.14	98.78	98.86
2:0.1		2527.32	6.27	97.36	94.07
3:0.1		2446.18	10.33	95.62	91.61
1:0.1	80	2012.41	3.38	98.13	98.30
2:0.1		1976.17	7.47	95.96	94.55
3:0.1		1968.45	12.17	93.51	92.83

The composition of the recovered lithium hydroxide solution was quantified by two-end-point acid–base titration using standardized 0.1 M HCl under potentiometric control. The first end point (EP_1, ≈pH 8.3) corresponds to complete neutralization of OH^- and half-neutralization of CO_3^{2-}:

$$OH^- + H^+ \rightarrow H_2O,\ CO_3^{2-} + H^+ \rightarrow HCO_3^-$$

The second end point (EP_2, ≈pH 3.5) corresponds to neutralization of the remaining HCO_3^-:

$$HCO_3^- + H^+ \rightarrow H_2CO_3\ (aq)\ (\rightarrow CO_2 + H_2O)$$

Let V_1 and V_2 (mL) be the volumes of 0.1 M HCl consumed at EP_1 and EP_2, respectively, and let mmm (g) be the sample mass subjected to titration. From the carbonate–hydroxide stoichiometry, the moles of CO_3^{2-} and OH^- in the sample are

$$n_{CO_3^{2-}} = \frac{0.1(V_2 - V_1)}{1000},\ n_{OH} = \frac{0.1(2V_1 - V_2)}{1000}$$

Multiplying by the molar masses of Li_2CO_3 (73.8882 g mol^{-1}) and LiOH (23.940 g mol^{-1}), the mass fractions (wt.%) of Li_2CO_3 and LiOH in the product are obtained as Equations (16) and (17):

$$Li_2CO_3(wt.\%) = \frac{0.1(V_2 - V_1)}{1000}\frac{73.8882}{m} \times 100 \quad (16)$$

$$LiOH(wt.\%) = \frac{0.1(2V_1 - V_2)}{1000}\frac{23.940}{m} \times 100 \quad (17)$$

Table 5 compiles the titration-derived and contents (both in g L^{-1} and wt.%) for at 60, 70, and 80 °C. The LiOH fraction increases with temperature, while the fraction decreases, indicating suppressed carbonation and improved stabilization of the hydroxide at elevated temperatures. The dependence on is weak within 1–3, implying that once stoichiometric hydroxide is provided and is precipitated, additional OH^- does not noticeably shift the composition. The highest LiOH content was obtained at 70 °C, yielding 90.29 wt.% LiOH (9.71 wt.%). These results are consistent with the Eh–pH stability analysis (Section 3.4), which places the product solutions in the domain under alkaline, non-oxidizing conditions, and with the process controls (vacuum–Ar handling) that minimize CO_2 ingress and consequent carbonation.

Table 5. Results of two-end-point pH titration of the recovered LiOH solutions at different temperatures and $[OH^-]/[Li^+]$ ratios.

Temperature, °C	[OH]:[Li] mol Ratio	LiOH, g/L	Li_2CO_3, g/L	LiOH, %	Li_2CO_3, %
60	1	3.875	0.9381	86.43	13.57
	2	3.705	0.9038	86.34	13.66
	3	3.584	0.8136	87.17	12.83
70	1	4.275	0.7097	90.29	9.71
	2	4.025	0.7424	89.32	10.68
	3	3.942	0.6884	89.83	10.17
80	1	4.248	0.7111	90.21	9.79
	2	4.077	0.6981	90.01	9.99
	3	3.964	0.7438	89.16	10.84

Based on the conversion, recovery, and titration analyses, the optimal reaction condition for producing lithium hydroxide was identified as 70 °C with $[OH^-]/[Li^+]$ = 1. Under this condition, the post-reaction filtrate was evaporated at ≥90 °C for 24 h under a vacuum–Ar atmosphere to suppress carbonation and promote crystallization of lithium hydroxide monohydrate ($LiOH{\cdot}H_2O$). The XRD pattern of the evaporatively crystallized powder (Figure 17) displays reflections that can be indexed to $LiOH{\cdot}H_2O$ together with LiOH, indicating co-existence of the monohydrate and anhydrous hydroxide phases after drying at 90 °C. No additional crystalline phases were detected within the instrumental limits, which is consistent with the process design (inert atmosphere, low CO_2 activity) that minimizes formation of parasitic carbonates during evaporation and handling.

The XRD of the separated precipitate obtained after vacuum filtration (Figure 18) shows a single-phase $BaSO_4$ pattern. This confirms the high selectivity of the double decomposition route—sulfate is captured as an insoluble barite phase (low Ksp), which thermodynamically drives Li_2SO_4 conversion to LiOH and simultaneously facilitates solid–liquid separation. Elemental analysis by ICP-OES of the crystallized $LiOH{\cdot}H_2O$ indicates a purity of 99.8%, with only trace impurities at or below typical quantification limits. Considering the phase assemblage observed by XRD, further controlled dehydration/crystallization

during the evaporation step (still under vacuum–Ar to avoid CO_2 uptake) is expected to increase the fraction of anhydrous LiOH and thus further improve product purity. Under the selected operating window (60–80 °C; $[OH^-]/[Li^+] \approx 1$), impurity speciation follows hydroxide/sulfate equilibria. Al^{3+} and Fe^{3+} precipitate as hydroxides and partition into the $BaSO_4$ cake; Ca^{2+} and Mg^{2+} show limited solubility at high pH and are partly rejected as hydroxides. Increasing $[OH^-]/[Li^+] > 2$ raised slurry viscosity and favored $BaSO_4$ occlusion, lowering Li recovery. Monovalent Na^+/K^+ remain primarily in solution and are minimized by cake washing and by low-CO_2 crystallization. With these controls, the crystallized $LiOH{\cdot}H_2O$ achieved ~99.8 wt.% purity by ICP-OES, and XRD showed no foreign crystalline phases.

3.5. Overall Advantages, Limitations, and Comparison with Prior Routes

Lithium hydroxide can be produced from secondary or intermediate Li sources by several established routes. Calcium hydroxide precipitation from Li_2SO_4 or LiCl feeds removes sulfate as $CaSO_4$, but the formation of gypsum scales and the relatively modest selectivity to LiOH at comparable temperatures remain well-known drawbacks. A second family of processes proceeds via Na_2CO_3 carbonation to Li_2CO_3 followed by causticization with $Ca(OH)_2$ or NaOH; while effective, this pathway introduces an additional CO_2 loop and typically requires two solid–liquid separations, increasing complexity and consumables. A third option employs direct brine or electrochemical schemes (e.g., chlor-alkali-coupled or membrane-assisted configurations), which can achieve high purities but demand tight impurity control and dedicated electrolyzer infrastructure [24,25]. In contrast, the $Ba(OH)_2$ double-decomposition developed here converts a Li_2SO_4-rich feed at moderate temperatures (60–80 °C) and is thermodynamically driven by the formation of sparingly soluble $BaSO_4$. Under the $[OH^-]/[Li^+]$ window identified experimentally, sulfate removal approaches completeness and LiOH selectivity is high, while the route avoids a CO_2 throughput and minimizes intermediate conversions. The resulting $LiOH{\cdot}H_2O$ attains ~99.8 wt.% with impurity levels compatible with battery-grade specifications, and $BaSO_4$ is produced as a single, easily filterable phase. Operation within this mild thermal window limits energy input and obviates high-temperature caustic roasting. Moreover, multivalent cations such as Al^{3+}, Fe^{3+}, Ca^{2+}, and Mg^{2+} are largely rejected into the $BaSO_4$-rich residue or hydroxide side-solids under alkaline conditions, yielding a clean LiOH solution prior to crystallization. Low-CO_2 handling—sealed vessels, glove-box subsampling, and vacuum/argon evaporation—further suppresses parasitic carbonation, as corroborated by titration-based speciation. The approach nonetheless entails specific trade-offs. The use of Ba reagents requires careful management at scale, including cost, regulatory handling, and potential valorization of the barite by-product. At high $[OH^-]/[Li^+]$ ratios, hydrodynamic effects become non-negligible: increased viscosity and $BaSO_4$ occlusion depress Li recovery, which motivates operation near $[OH^-]/[Li^+] \approx 1$ within the identified process window. In addition, industrial Li_2SO_4 feeds exhibit variability in Na^+, K^+, Ca^{2+}, and Mg^{2+}, suggesting that guard-polishing or simple pretreatments may be warranted to stabilize specifications. Finally, the kinetics and optimization of the upstream leaching step were outside the scope of this study because the Li-bearing feed was supplied industrially; a complete techno-economic and life-cycle assessment that includes upstream operations is an important direction for future work. From an industrial perspective, the large inventory of Li captured in spent saggers and other sulfate-bearing intermediates makes this short flowsheet—$Li_2SO_4 \rightarrow LiOH{\cdot}H_2O$—attractive. The combination of high selectivity, mild temperature, robust impurity rejection, and carbonation control provides a complementary alternative to Ca-based and CO_2-intensive routes, and supports practical integration into recycling-compatible hydrometallurgical schemes.

4. Conclusions

This study demonstrates a hydrometallurgical route to producing high-purity lithium hydroxide monohydrate ($LiOH{\cdot}H_2O$) starting from lithium sulfate monohydrate ($Li_2SO_4{\cdot}H_2O$). Crystal water was first removed by thermal dehydration to form anhydrous Li_2SO_4, after which a double-decomposition reaction with $Ba(OH)_2$ was employed. The post-reaction filtrate was finally evaporated at $\geq$90 °C for 24 h. under a vacuum–Ar atmosphere to suppress carbonation and crystallize $LiOH{\cdot}H_2O$ powder.

1. Thermal dehydration. $Li_2SO_4{\cdot}H_2O$ was converted to Li_2SO_4 + H_2O at 300 °C for 2 h (Ar, MgO crucible), as confirmed by XRD. No parasitic phases from crucible reactions were detected, verifying that the dehydration step proceeds cleanly under the selected conditions.

2. Double decomposition and solution chemistry. Using $Ba(OH)_2$, the effects of reaction temperature (60/70/80 °C) and $[OH^-]/[Li^+]$ molar ratio (1/1, 2/1, 3/1) were quantified. Higher temperature increased both conversion and recovery, while excess OH^- ($\geq$2/1) led to gradual decreases, attributable to viscosity/filtration penalties and unnecessary reagent excess. Measured pH–Eh values for all conditions resided within the Li–Ba–S–H_2O Eh–pH stability field consistent with LiOH(aq) and $BaSO_4$(s) domains. Two-end-point titration showed that the LiOH fraction increased with temperature and was only weakly dependent on $[OH^-]/[Li^+]$ in the range 1–3.

3. Optimal condition and product quality. The optimum within the tested space was 70 °C, $[OH^-]/[Li^+]$ = 1, yielding conversion 98.78%, Li recovery 98.86%, and a LiOH content of 90.29 wt.% in solution by titration. The final powder obtained by vacuum–Ar evaporation exhibited $LiOH{\cdot}H_2O$ (with LiOH) reflections in XRD, while the separated precipitate was single-phase $BaSO_4$, evidencing high selectivity of the double-decomposition step. ICP-OES confirmed 99.8% purity for the crystallized $LiOH{\cdot}H_2O$. Further controlled dehydration during evaporation (still under CO_2-free conditions) is expected to increase the anhydrous LiOH fraction if desired.

Overall, the coupled sequence—thermal dehydration of $Li_2SO_4{\cdot}H_2O$, $Ba(OH)_2$-driven double decomposition, and CO_2-free evaporation—enables the efficient production of high-purity $LiOH{\cdot}H_2O$. Given the role of $LiOH{\cdot}H_2O$ as a key precursor for high-Ni cathode materials, these findings provide a practical basis for reliable, domestic $LiOH{\cdot}H_2O$ supply via recycling-compatible chemistry and may serve as a foundation for industrial scale-up.

Author Contributions: S.H.: Methodology, Data curation, Investigation, Writing—original draft, Data curation, Software, Validation; J.-P.W.: Project administration, Conceptualization, Writing—review and editing, Funding acquisition. All authors have read and agreed to the published version of the manuscript.

Funding: This work was supported by the Renewable Energy R&D program (Grant No. 20229A10100100) funded By the Ministry of Trade, Industry & Energy (MOTIE, Republic of Korea).

Data Availability Statement: The original contributions presented in the study are included in the article, further inquiries can be directed to the corresponding author.

Conflicts of Interest: The authors declare no conflicts of interest.

References

1. Grageda, M.; Gonzalez, A.; Quispe, A.; Ushak, S. Analysis of a Process for Producing Battery Grade Lithium Hydroxide by Membrane Electrodialysis. *Membranes* **2020**, *10*, 198. [CrossRef]
2. Kim, S.Y.; Choi, S.H.; Lee, E.J.; Kim, J.S. Synthesis and electrochemical performance of Ni-rich NCM cathode materials for lithium-ion batteries. *J. Korean Electrochem. Soc.* **2017**, *20*, 67. [CrossRef]
3. Ngala, J.K.; Chernova, N.A.; Ma, M.; Mamak, M.; Zavalij, P.Y.; Whittingham, M.S. The synthesis, characterization and electrochemical behavior of the layered $LiNi_{0.4}Mn_{0.4}Co_{0.2}O_2$ compound. *J. Mater. Chem.* **2004**, *14*, 214. [CrossRef]

4. Kim, D.W.; Park, J.R.; Ahn, N.K.; Choi, G.M.; Jin, Y.H.; Yang, J.K. A review on the recovery of the lithium carbonate powders from lithium-containing substances. *J. Korean Cryst. Growth Cryst. Technol.* **2019**, *29*, 91. [CrossRef]
5. Hien-Dinh, T.T.; Luong, V.T.; Giere, R.; Tran, T. Extraction of lithium from lepidolite via iron sulphide roasting and water leaching. *Hydrometallurgy* **2015**, *153*, 154. [CrossRef]
6. Ryabtsev, A.D.; Nemkov, N.M.; Kotsupalo, N.P.; Serikova, L.A. Preparation of high-purity lithium hydroxide monohydrate from technical-grade lithium carbonate by membrane electrolysis. *Russ. J. Appl. Chem.* **2004**, *77*, 1108–1116. [CrossRef]
7. Kim, G.J. Recovery of lithium hydroxide from spent lithium carbonate using crystallizations. *Sep. Sci. Technol.* **2008**, *43*, 420–430. [CrossRef]
8. Yuan, B.; Wang, J.; Cai, W.; Yang, Y.; Yi, M.; Xiang, L. Effects of temperature on conversion of Li_2CO_3 to LiOH in $Ca(OH)_2$ suspension. *Particuology* **2017**, *34*, 97–102. [CrossRef]
9. Joo, S.Y.; Kang, Y.B.; Shim, H.W.; Byun, S.H.; Kim, Y.H.; Lee, C.G.; Kim, D.G. Study on preparation of high purity lithium hydroxide powder with 2-step precipitation process using lithium carbonate recovered from Waste LIB battery. *J. Korean Inst. Resour. Recycl.* **2019**, *28*, 60–67. [CrossRef]
10. Kumar, A.; Fukuda, H.; Hatton, T.A. Lithium Recovery from Oil and Gas Produced Water: A Need for a Growing Energy Industry. *ACS Energy Lett.* **2019**, *4*, 1471–1474. [CrossRef]
11. Tam, T.; Luong, V.T. Ch. 3 Lithium Production Process. In *Lithium Process Chemistry—Resources, Extraction, Batteries, and Recycling*; Chagnes, A., Swiaatowska, J., Eds.; Elsevier Inc.: New York, NY, USA, 2015; p. 99.
12. Chon, U.; Han, G.; Kim, K. Current Status of Lithium Resources. *J. Korean Inst. Resour. Recycl.* **2010**, *19*, 3–8. Available online: https://koreascience.kr/article/JAKO201029848352569.page (accessed on 18 November 2025).
13. Meng, F.; McNeice, J.; Zadeh, S.S. Review of Lithium Production and Recovery from Minerals, Brines, and Lithium-Ion Batteries. *Miner. Process. Extr. Metall. Rev.* **2021**, *42*, 123–141. [CrossRef]
14. Yanjia, Z.; Xiaodong, T.; Dayong, Q.; Jingjing, L.; Hong, W. Research progress of technology of lithium extraction. *Separ. Purif. Tech.* **2025**, *359*, 130561. [CrossRef]
15. Rioyo, J.; Tuset, S.; Grau, R. Lithium extraction from spodumene by the traditional sulfuric acid process: A review. *Miner. Process. Extr. Metall. Rev.* **2020**, *46*, 1–10. [CrossRef]
16. Garrett, D.E. *Handbook of Lithium and Natural Calcium Chloride*; Elsevier Science & Technology: Amsterdam, The Netherlands, 2004; p. 164.
17. David, L. Experimental phase equilibria in the system $LiAlSiO_4$-SiO_2-H_2O: A petrogenetic grid for lithium- rich pegmatites. *Am. Mineral.* **1984**, *69*, 995–1004.
18. Zilberman, P. The CO_2 Absorber Based on LiOH. *Acta Med. Marisiensis.* **2015**, *61*, 4–6. [CrossRef]
19. Liu, H.; Azimi, G. Production of battery grade lithium hydroxide monohydrate using barium hydroxide causticizing agent. *Resour. Conserv. Recycl.* **2022**, *179*, 106115. [CrossRef]
20. Neuman, S.P. Theoretical derivation of Darcy's law. *Acta Mech.* **1977**, *25*, 153–170. [CrossRef]
21. Li, J.; Zeng, T.; Kobayashi, N.; Wu, R.; Xu, H.; Deng, L.; He, Z.; Huang, H. Carbonation Reaction of Lithium Hydroxide during Low-Temperature Thermal Energy Storage. *J. Renew. Mater.* **2021**, *9*, 1621–1630. [CrossRef]
22. Aprilianto, D.R.; Perdana, I.; Rochmadi Petrus, H.T.B.M. Effect of Sulfate and Carbonate Ions on Lithium Carbonate Precipitation. *Ind. Eng. Chem. Res.* **2024**, *63*, 18262–18273. [CrossRef]
23. Vera, M.L.; Torres, W.R.; Galli, C.I.; Chagnes, A.; Flexer, V. Environmental impact of direct lithium extraction from brines. *Nat. Rev. Earth Environ.* **2023**, *4*, 675–690. [CrossRef]
24. Wei, G.; Wang, M.; Lin, C.; Xu, C.; Gao, J. Optimizing Operational Parameters for Lithium Hydroxide Production by Bipolar Membrane Electrodialysis. *Separations* **2024**, *11*, 146. [CrossRef]
25. Peeters, N.; Tijink, M. Conversion of Lithium Chloride into Lithium Hydroxide: A Literature Review. *J. Sustain. Metall.* **2024**, *10*, 1127–1145. [CrossRef]

Disclaimer/Publisher's Note: The statements, opinions and data contained in all publications are solely those of the individual author(s) and contributor(s) and not of MDPI and/or the editor(s). MDPI and/or the editor(s) disclaim responsibility for any injury to people or property resulting from any ideas, methods, instructions or products referred to in the content.